

The Pursuit of Engineering the Ideal Heart Valve Replacement or Repair

3D Printed Modeling of the Mitral Valve for Catheter-Based Structural Interventions

MARIJA VUKICEVIC,¹ DANIEL S. PUPERI,² K. JANE GRANDE-ALLEN,² and STEPHEN H. LITTLE¹

¹Department of Cardiology, Houston Methodist Research Institute, Weill Cornell Medicine/Houston Methodist Hospital, 6550 Fannin Street, SM-677, Houston, TX 77030, USA; and ²Department of Bioengineering, Rice University, 6100 Main St., MS 142, Houston, TX 77005, USA

(Received 17 February 2016; accepted 7 June 2016; published online 20 June 2016)

Associate Editor Lakshmi Prasad Dasi oversaw the review of this article.

Abstract—As catheter-based structural heart interventions become increasingly complex, the ability to effectively model patient-specific valve geometry as well as the potential interaction of an implanted device within that geometry will become increasingly important. Our aim with this investigation was to combine the technologies of high-spatial resolution cardiac imaging, image processing software, and fused multi-material 3D printing, to demonstrate that patient-specific models of the mitral valve apparatus could be created to facilitate functional evaluation of novel trans-catheter mitral valve repair strategies. Clinical 3D transesophageal echocardiography and computed tomography images were acquired for three patients being evaluated for a catheter-based mitral valve repair. Target anatomies were identified, segmented and reconstructed into 3D patient-specific digital models. For each patient, the mitral valve apparatus was digitally reconstructed from a single or fused imaging data set. Using multi-material 3D printing methods, patient-specific anatomic replicas of the mitral valve were created. 3D print materials were selected based on the mechanical testing of elastomeric TangoPlus materials (Stratasys, Eden Prairie, Minnesota, USA) and were compared to freshly harvested porcine leaflet tissue. The effective bending modulus of healthy porcine MV tissue was significantly less than the bending modulus of TangoPlus ($p < 0.01$). All TangoPlus varieties were less stiff than the maximum tensile elastic modulus of mitral valve tissue (3697.2 ± 385.8 kPa anterior leaflet; 2582.1 ± 374.2 kPa posterior leaflet) ($p < 0.01$). However, the slopes of the stress-strain toe regions of the mitral valve tissues (532.8 ± 281.9 kPa anterior leaflet; 389.0 ± 156.9 kPa posterior leaflet) were not different than those of the Shore 27, Shore 35, and Shore 27 with Shore 35 blend TangoPlus material ($p > 0.95$). We have demonstrated that patient-specific mitral valve models can be reconstructed

from multi-modality imaging datasets and fabricated using the multi-material 3D printing technology and we provide two examples to show how catheter-based repair devices could be evaluated within specific patient 3D printed valve geometry. However, we recognize that the use of 3D printed models for the development of new therapies, or for specific procedural training has yet to be defined.

Keywords—Heart valve modeling, Percutaneous mitral valve repair, 3D printing, MitraClip.

ABBREVIATIONS

| | |
|--------|--|
| CT | Computed tomography |
| DICOM | Digital imaging and communication in medicine |
| IPS | Image processing software |
| LA | Left atrium |
| LV | Left ventricle |
| MR | Mitral regurgitation |
| MV | Mitral valve |
| 3D TEE | Three-dimensional transesophageal Echocardiography |
| TMVR | Trans-catheter mitral valve replacement |

INTRODUCTION

Mitral valve regurgitation (MR) is one of the most common heart disorders and its prevalence increases with patient age.¹⁰ Although a surgical repair or replacement of the mitral valve is a primary treatment for symptomatic severe MR, for the very elderly patients or those with significant comorbidities, the

Address correspondence to Stephen H. Little, Department of Cardiology, Houston Methodist Research Institute, Weill Cornell Medicine/Houston Methodist Hospital, 6550 Fannin Street, SM-677, Houston, TX 77030, USA. Electronic mail: shlittle@tmhs.org

risk of surgical valve intervention is too great. Increasingly, catheter-based repair of the mitral valve is being considered for such patients. Today the catheter-based repair of MR is limited to: (1) the use of the MitraClip system to create a fixed coaptation of the two mitral leaflets (Abbott Vascular, Abbott Park, IL);⁴ (2) the use of a vascular closure devices to occlude a mitral leaflet perforation;^{3,5} and (3) early trials and ongoing development of trans-catheter mitral valve replacement (TMVR) devices.⁴ The typical procedural stages of a MitraClip deployment are shown in Fig. 1. A principal limitation of each of the trans-catheter mitral treatments is our current inability to accurately predict how the repair or replacement device will interact with complex native and pathologic geometry of the patient, and how well the device will achieve the treatment goal—namely the elimination or significant reduction of MR.

The development of patient-specific 3D models of the mitral valve complex may impact the field of trans-catheter valve intervention in several important ways. A clinical team of physicians could interact with a specific patient model prior to a proposed catheter-based treatment to guide selection of the most appropriate device; to alter the implantation protocol based on an evaluation of the anatomic “landing zone”;⁵ to request additional invasive or non-invasive imaging prior to the intervention; or simply to gain a 3D volumetric perspective to aid in the prediction of device/patient functional success or failure. As catheter-based structural heart interventions become increasingly complex, the ability to effectively model patient-specific valve geometry as well as the interaction of an implanted device within that geometry will become increasingly important.^{5,7,8}

3D printing is a fabrication technique for transferring 3D digital objects into physical models and these techniques have recently been used to create specific cardiac structural pathologies.^{7,8} Such models are

typically created from computed tomography (CT) imaging data. However 3D transesophageal echocardiographic (TEE) imaging has recently been used as a data source for 3D printing of the mitral valve leaflets and annulus morphology.^{2,6,11,13}

Our aim with this investigation was to combine the technologies of high-spatial resolution cardiac imaging, image processing software (IPS), and fused multi-material 3D printing, to demonstrate that patient-specific models of the mitral valve apparatus could be created to facilitate functional evaluation of novel trans-catheter mitral valve repair strategies.

MATERIALS AND METHODS

Image Acquisition and Segmentation

Reconstruction of target MV geometry began by acquiring high quality images using both 3D TEE (iE33, Philips ultrasound, Andover, MI) and cardiac CT (Force, Siemens, Germany) for three patients with significant MR prior to a planned catheter-based mitral repair procedure. Informed patient consent was acquired and our institutional review board approved the study. Volumetric data was exported in digital imaging and communication in medicine (DICOM) format from both imaging modalities and imported into IPS (Mimics Medical 18.0 × 64 for CT images processing and Mimics Research 18.0 × 64 for 3D TEE images processing, Materialize, USA), which contains software tools for the identification of target cardiac anatomy, region-of-interest segmentation, specific tissue tagging, and data export features.

From 3D TEE, an en-face mid-esophageal diastolic data set of the mitral leaflets was acquired which contained 208 slices with resolution of 176×211 , pixel size of 0.548 mm, and slice increment of 0.484 mm. An additional imaging long-axis 3D TEE data set was acquired that included the entire ventricular volume

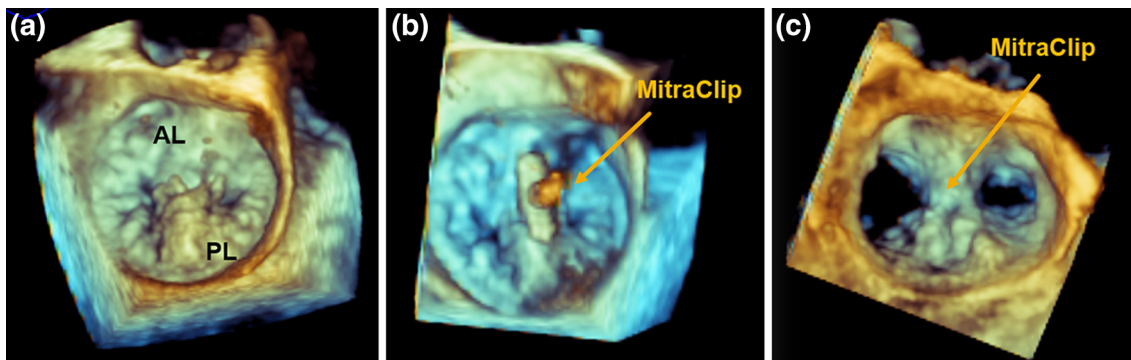


FIGURE 1. Catheter-based mitral valve repair. (a) 3D TEE image of regurgitant mitral valve (MV) prior to MitraClip procedure. (b) 3D TEE image of the MitraClip deployment during the percutaneous MV repair. (c) 3D TEE image of repaired MV with implanted MitraClip device; anterior leaflet (AL), posterior leaflet (PL).

within 208 slices with resolution of 176×183 , pixel size of 0.78 mm and slice increment of 0.625 mm. From CT imaging the acquired data set was taken at the 30% R-R wave interval and contained 472 slices with resolution of 512×512 , pixel size of 0.422 mm, slice increment of 0.5 mm and slice thickness of 1 mm.

The 3D volumetric imaging data was reassembled into three 2D image planes (coronal, sagittal and axial) in which the target anatomy was identified and the segmentation region of interest was created based on the threshold intensity of pixels. It included the segmented inner region and the boundaries of the specific anatomic structures (muscle, soft tissue, blood volume or calcified structures), as shown in Figs. 2, 3 and 6. Non-cardiac anatomic data was manually eliminated (see segmentation panel in Figs. 2, 3, and Fig. 6). The valve anatomy of interest was manually identified and digitally tagged throughout the entire imaging volume then rendered into a 3D digital model (Figs. 2c, 2d, and 3). Tagged anatomic surfaces were reviewed to ensure that local structural features did not intersect or overlap inappropriately and that no contiguous surface was incomplete. The model was then saved as an STL file and exported for 3D printing.

Replication of Valve Leaflets and Annulus

From the volumetric imaging data, the mitral leaflets were identified, segmented and anatomically tagged using sagittal and coronal diastolic views (see

Fig. 2). The mitral annulus was identified as the location where the leaflets meet the atrial and ventricular walls. The detailed geometry of the mitral apparatus was manually identified and tagged using multiple rotational views. The segmented anatomic data was rendered into a 3D digital model as shown in Fig. 3d. The pathological depositions of calcium were replicated and integrated within the posterior leaflet (yellow structure in Figs. 3d and 3e). The ventricular volume was reconstructed from the same imaging data set, along with the myocardial structure, LV outflow tract and the left atrium (LA), as shown in Fig. 3c.

Selection and Testing of Material Properties

To guide the selection of appropriate materials for the 3D printing, we first compared the flexural and tensile material behavior of several print material samples to that of freshly harvested porcine mitral valve tissue (Fig. 4a). We evaluated the mechanical properties of several samples of an elastomeric material (TangoPlus, Stratasys, Eden Prairie, Minnesota) that is available in a range of hardness (Shore values). Test strips 5 mm wide \times 30 mm long \times 2 mm thick ($n = 4$) were cut from TangoPlus samples of Shore value 27, 35, and 60 and from a 3D printed dual-material combination of Shore 27 and 35 (as described below) for the mechanical testing, as shown in Fig. 4b. Mitral valve leaflets were dissected from healthy 6-9 month old porcine hearts obtained from a local

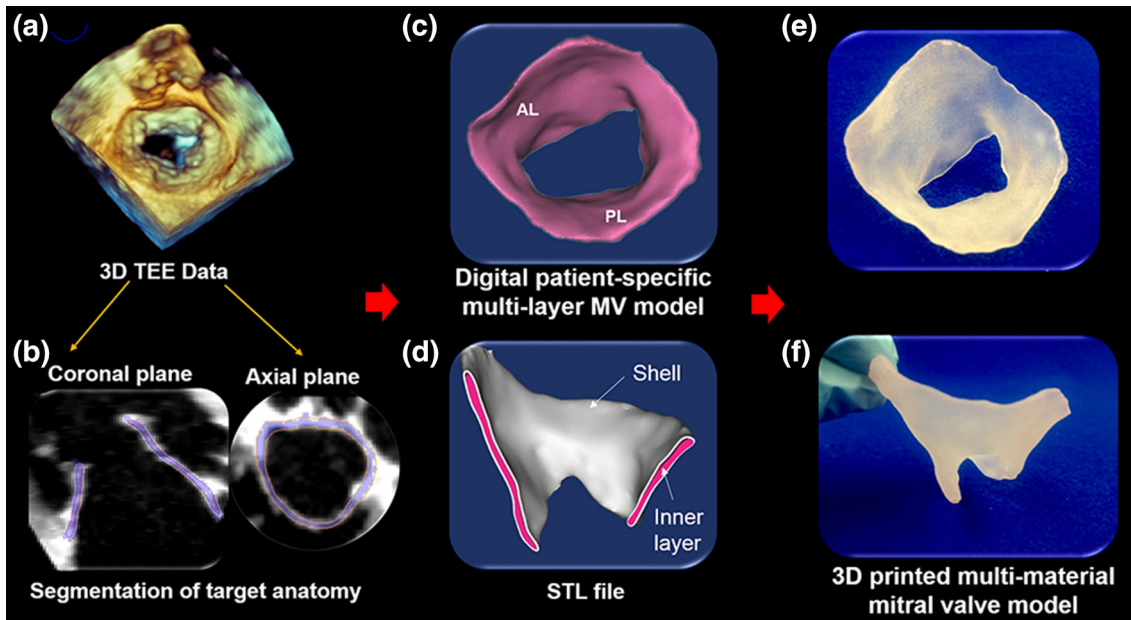


FIGURE 2. Mitral valve reconstruction from 3D TEE images. (a) 3D TEE en-face imaging data set. (b) 2D imaging planes derived from 3D TEE data with superimposed segmentation mask over the MV leaflets. (c) Digital model of patient-specific valve. (d) Cross section of the digital valve model including the outer shell (white) and inner structure (pink). (e) En-face photo of the 3D printed MV model. (f) Lateral view on the 3D printed MV model.

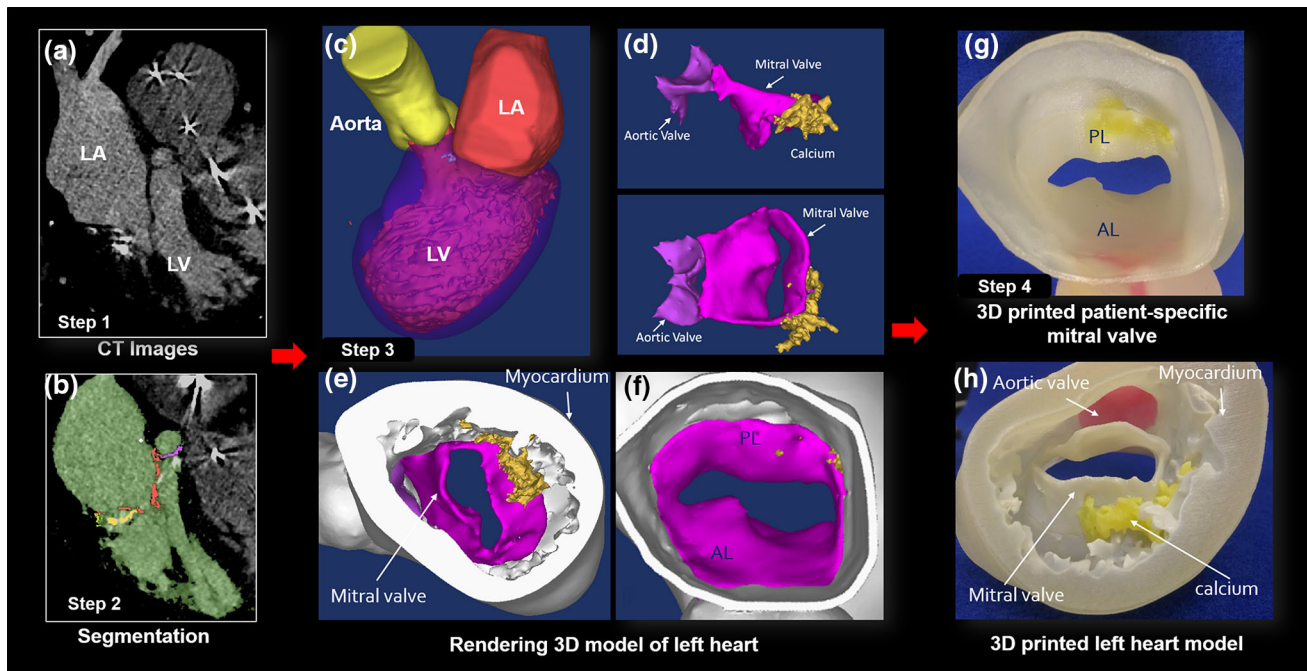


FIGURE 3. Mitral valve reconstruction from CT images. (a) CT imaging data set. (b) Identified and segmented geometry of left heart, including aortic valve, mitral valve and calcium depositions. (c) LV, Aortic and LA 3D rendered volume. (d) Lateral and en-face view on the reconstructed MV, aortic valve and calcium. (e) Apical view on MV and intraventricular structures. (f) MV integrated with left heart model. (g) En-face view on 3D printed MV model integrated in the left heart. (h) Apical view on the 3D printed multi-material model of MV and intraventricular structures.

commercial abattoir (Fisher Ham and Meats, Spring, TX). Radially-oriented rectangular strips 5 mm wide \times 15 mm long were cut from both the posterior and anterior leaflets ($n = 3$) as shown in Fig. 4a. The flexural properties of the porcine leaflet sections and TangoPlus material were characterized using a custom built 3-point bending tester as previously described.¹ Strips were deformed by a flexure bar of known elastic modulus to force the material to bend (Figs. 4c and 4d). Custom Python scripts were used to calculate the effective bending modulus by automated video image analysis. The effective bending modulus was defined by linear regression of the curvature of the material compared to its bending moment as previously described,^{1,9} using Euler–Bernoulli beam theory. The relationship between the applied bending moment, M , and the curvature of the material $\frac{d^2v}{dx^2}$ is described by the equation: $M = E_{\text{eff}}I\frac{d^2v}{dx^2}$, where I is the moment of inertia of the beam cross section and E_{eff} is the effective bending modulus. The effective bending modulus was calculated by dividing the slope of the applied moment vs. curvature line by the moment of inertial, I . The bending behavior of the porcine mitral leaflet segments was measured in two ways, both with the natural curvature (towards atrialis layer) and against the natural curvature (towards ventricularis layer).

After being tested in bending, the same strips of mitral leaflets and TangoPlus material were tested in uniaxial tension using a Bose ELF 3200 mechanical tester (Bose Electroforce, Eden Prairie, MN). After preconditioning, samples were elongated to failure at a rate of 0.2 mm/s (Fig. 4). For porcine leaflet samples, an elastic modulus was calculated for both the toe region (the region of the initial material deformation under the initial mechanical testing load, equivalent with the collagen fibers uncrimping in the mitral tissue), and the stiffer collagen-stretching region. The elastic modulus of the toe region was defined as the slope of the linear regression of the stress vs. strain curve from 1 to 15% strain. The elastic modulus of the collagen region was calculated by finding the maximum slope of the stress vs. strain curve that encompassed at least 5% strain. For the TangoPlus materials, the elastic modulus was calculated by linear regression of the stress vs. strain curve.

The mitral leaflets were designed as a bi-layer of two different print materials. The outer shell was printed with a 0.4 mm thick layer of the relatively soft material TangoPlus, Shore 27. By subtracting the outer shell from the original digital model we obtained the inner structure of the valve (see Fig. 2d) and in that way separated two layers of the valve. The inner layer was printed using a medium-soft TangoPlus material, Shore 35 (Stratasys, Eden Prairie, Minnesota), with

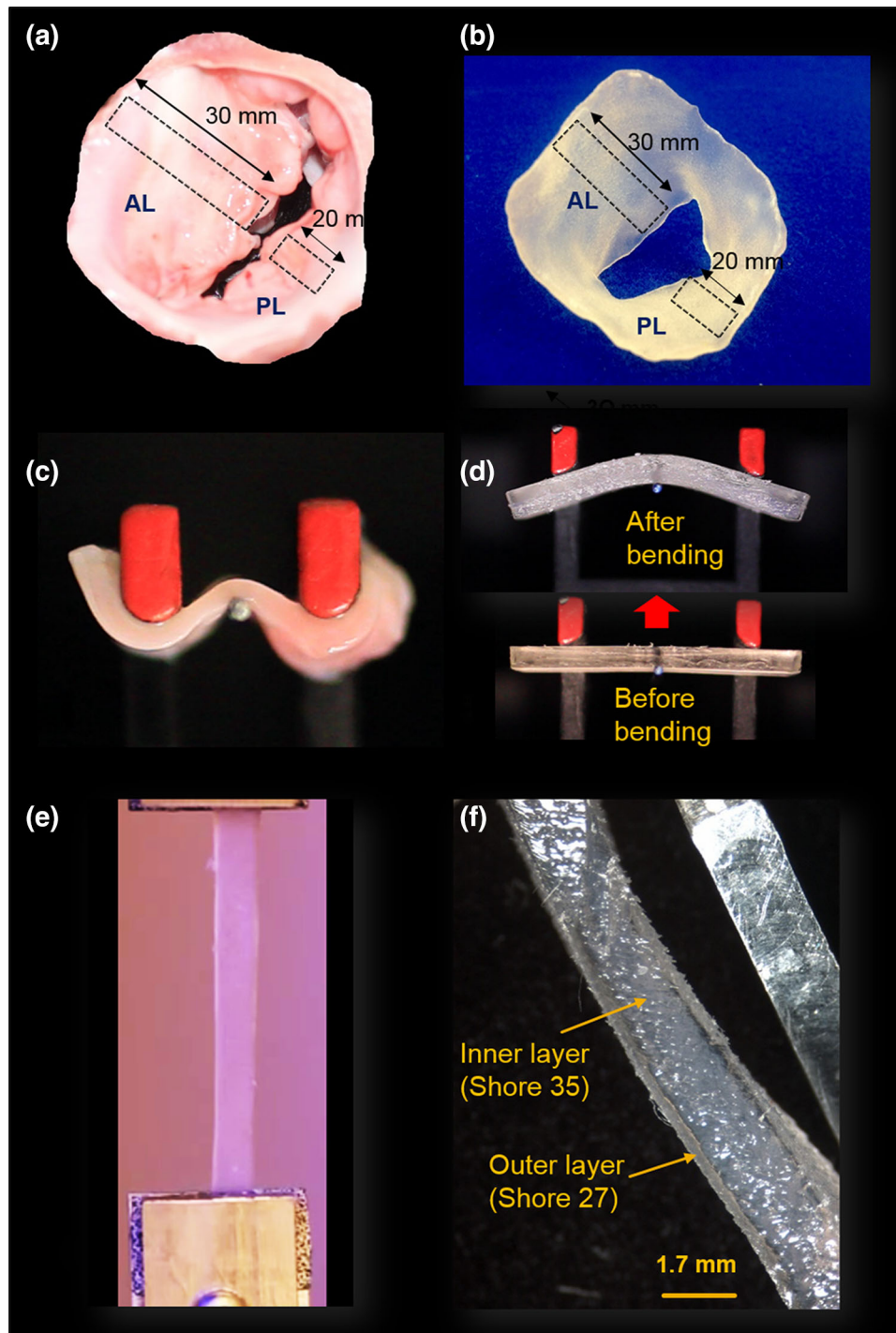


FIGURE 4. Mechanical material testing. (a) Porcine mitral valve as a reference control for mechanical testing of MV materials. (b) Dual-material 3D-printed MV model used for mechanical testing of material. (c) Mitral tissue after bending test. (d) TangoPlus material sample before and after the bending test. (e) Stretched TangoPlus material sample during the tension testing. (f) Microscopic image of cross section of multi-layer anterior leaflet demonstrating that the core of the leaflet was fabricated of stiffer material (TangoPlus-Shore 35), while the surface layer was 3D printed of softer material (TangoPlus-Shore 27).

thickness defined by the remaining leaflet cross-sectional diameter after subtracting the thickness of the two outer print layers. The surrounding LA and LV tissue was replicated using TangoPlus (Shore 27)

material, the papillary muscle was replicated using slightly harder TangoPlus (Shore 60), and the pathologic calcium deposits were printed using very hard VeroWhite material (see Figs. 3g and 3h).

Reconstruction of Subvalvular Apparatus

The subvalvular functional elements of the mitral valve were initially identified from a 3D TEE data set (see Fig. 5a). After identifying the elements of subvalvular apparatus including the geometry of the papillary muscles and the volume and contour of the LV cavity we created a segmentation region of interest of those functional elements. The anatomic tagging of the papillary muscles throughout the entire imaging volume required an interactive coordinate system within the IPS to allow us to choose an optimal view. The LV volume and geometry were also segmented from this data set (see Figs. 5a and 5b).

Since the chordae tendineae were not completely identified from 3D TEE images, we also explored whether CT images could be used for the reconstruction of the subvalvular apparatus including the chordae tendineae. Identification of the majority of the primary chordae tendineae required the manipulation of the CT volumetric imaging data using multiple off-axis rotational planes (Fig. 6, left panel).

Fusion of Anatomic Image Data

Short-axis 3D TEE images of the mitral leaflets (see Fig. 2c) as well as long-axis 3D TEE images containing the LV geometry were imported into the IPS. The orientation of the MV model with the long-axis of the LV was different for each image dataset, thus requiring a manual alignment of digital MV leaflet model with the digital LV model. The mitral annulus was present in both the en-face and long-axis 3D TEE data sets and thus provided the anatomic continuity for image co-registration. The MV geometry was fused with the LV

and papillary muscles into an integral digital model shown in Fig. 5b. The completed digital model was replicated into a physical 3D model (see Figs. 2e and 2f). We repeated this process using the 3D TEE data of the mitral valve leaflet geometry and annulus and fused it with the CT-derived data of the papillary muscles, chordae tendineae and LV geometry as shown in Fig. 6.

Benchmark Mitral Valve Structural Intervention

Two patient-specific models of the mitral valve were created to evaluate their potential utility for the planning of structural catheter-based interventions. For the first model a dual-material model was reconstructed from 3D TEE data (Fig. 2) and used for modeling of a MR repair procedure with the MitraClip system (see Fig. 8a). The MitraClip is made of two cobalt-chromium arms 8 mm long and 4 mm wide, coated with polyester fabric. The MitraClip device was implanted into the MV model from the atrial side. The grippers were positioned perpendicular to coaptation in the central region of the anterior and posterior leaflet (Fig. 8a). The MitraClip was deployed using the clinical implantation protocol where the device that makes a contact with the ventricular surface of the mitral leaflets, is pulled back to create tension against the leaflets, then gripper arms are lowered to contact the leaflets on the atrial side, then the device is closed to force leaflet closure from the ventricular side. For this study we performed a qualitative review of the ability of the device to grasp the 3D printed MV leaflets and to maintain sufficient force to create a fused central coaptation region (as it is accomplished with a clinical MitraClip implantation).

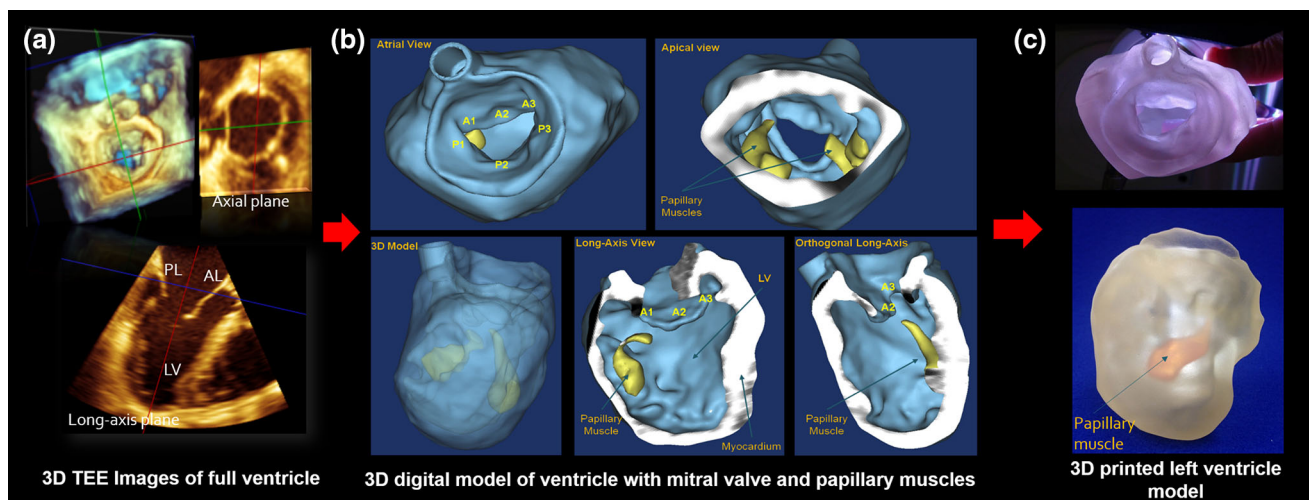


FIGURE 5. Assembling models from different data sets. (a) 3D TEE data set, shown with its en-face and long-axes view. (b) Digital model of left ventricle with papillary muscles reconstructed from long-axis 3D TEE data, integrated with MV reconstructed from en-face 3D TEE data set. Apical and long-axis cross-sectional view. (c) 3D printed patient-specific model of MV within LV with papillary muscles.

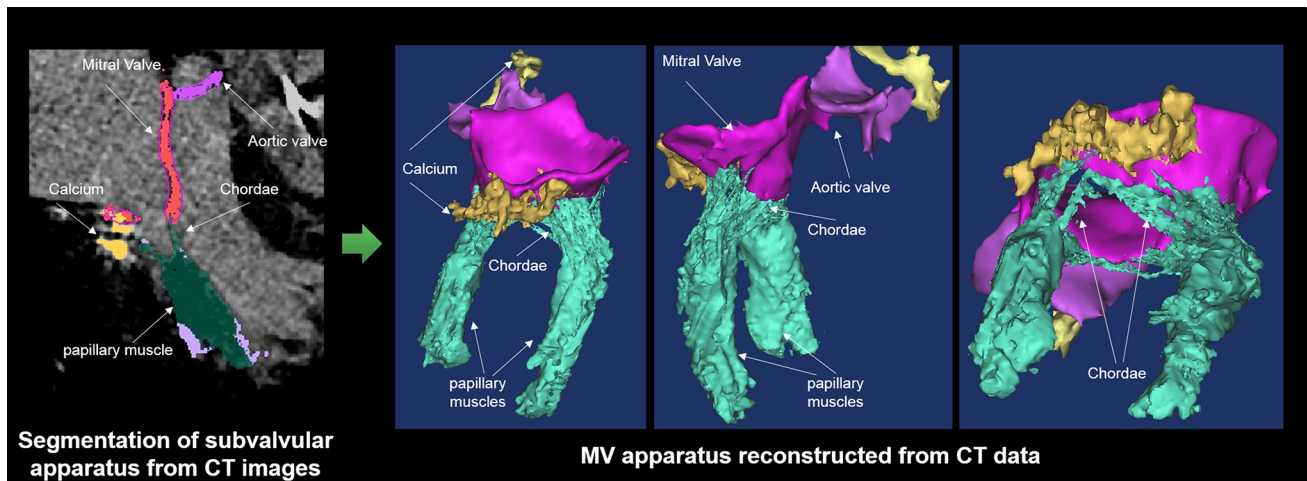


FIGURE 6. Reconstruction of subvalvular apparatus geometry, including the papillary muscles, calcium and chordae tendineae from CT images.

For the second model, a clinical case of mitral leaflet perforation as a consequence of local tissue infection, was replicated to evaluate whether a catheter-based repair procedure might be feasible using a commercially available device designed to occlude a congenital arterial shunt (specifically a patent ductus arteriosus defect), (ADO II, St. Jude Medical, St. Paul, Minnesota). The patient-specific MV geometry including pathological elements (calcification, thickening, and perforation of the posterior leaflet) was replicated, along with the surrounding anatomical structures including the myocardium, papillary muscles and LV outflow tract (see Fig. 8b). The model was reconstructed using systolic phase CT data.

To evaluate the geometric accuracy of the second 3D printed model, the length and the width of the leaflet perforation, as well as the distances from the edge of the perforation to the edge of the posterior leaflet and the annulus were measured in the digital model and compared to the same measurements in the physical 3D printed MV model. A catheter-based repair of the 3D printed anatomic defect was performed using a vascular occluder device (ADO II device; waist 6 mm; length 4 mm; disc diameter 12 mm) to plug the large perforation in the posterior leaflet model. The size of the device chosen for the benchtop leaflet repair was based on the shape and position of the perforation relative to structurally important regions (the leaflet coaptation zone) and pathologic elements (sub-valvular calcium), which were replicated within the 3D printed MV model.

RESULTS

Image Acquisition and Segmentation

Reconstruction of the LV volume with mitral valve leaflets and pathological elements, required the acqui-

sition of 3D TEE imaging data sets from different perspectives; en-face valve images for the MV leaflet visualization; and long-axis images that contained the entire LV volume and subvalvular elements. These separate DICOM files were successfully exported from the Philips ultrasound platform for further analysis and segmentation. In contrast, CT image data was exported as a single DICOM file of the entire mitral valve and sub-valvular apparatus.

Digital tagging of MV anatomy was performed manually, while the segmentation of the LV and LA was semi-automatic. 3D TEE images provided good spatial resolution of mitral valve leaflets and annulus, while the chordae tendineae and LV myocardial geometry were not as reliably detected. In contrast, CT images were able to depict functional elements of the MV leaflets and the subvalvular apparatus, including the myocardial structure, papillary muscles, chordae tendineae and pathologic calcium deposits.

Segmentation of the MV with supporting elements, including the ventricular chamber, myocardium and papillary muscles from 3D TEE data took approximately 12 h of meticulous work. In contrast the segmentation of the MV leaflets and subvalvular anatomy required approximately 20 h of labor when based on CT image data.

Replication of Mitral Valve Leaflets

MV leaflets and annulus geometry were replicated first as a digital multi-layer patient-specific MV model (see Fig. 2c). Within the reconstructed valve model we created the 0.4 mm thick surface layer that we assigned as an outer shell, preserving the patient-specific geometry of the valve. The inner structure was differentiated from the outer layer and occupied the inner

space of the valve model (see Fig. 2d). As a physical model the 3D printed leaflets were mechanically movable, allowing for bending and distortions. Using CT data we were able to reconstruct and 3D print the MV leaflets with regional calcific depositions along with the surrounding myocardial structure and left ventricular (LV) outflow tract (see Fig. 3).

Mechanical Testing of MV Material Properties

The effective bending modulus of healthy porcine MV tissue was significantly less than the bending modulus of TangoPlus ($p < 0.01$; Fig. 7b). The posterior leaflet of the porcine MV had an effective bending modulus of 44.54 ± 27.25 kPa with the natural curvature and an effective bending modulus of 102.71 ± 37.38 kPa against natural curvature of the leaflet. The anterior leaflet had an effective bending modulus of 37.83 ± 10.38 and 65.28 ± 28.37 kPa with and against the natural leaflet curvature, respectively. TangoPlus material had an effective bending moduli of 911.13 ± 44.94 kPa (Shore 27), 963.50 ± 27.65 kPa (Shore 27/Shore 35), and 1185.72 ± 51.56 kPa (Shore 35), which were all significantly different from each other ($p < 0.01$).

The Shore 60 TangoPlus material (1300.3 ± 140.4 kPa) was significantly stiffer in tension than Shore 27 (380.3 ± 11.1 kPa), Shore 35 (526.8 ± 30.2 kPa), and the Shore 27/Shore 35 blend (460.7 ± 21.2 kPa) ($p < 0.01$). All TangoPlus varieties were less stiff than the maximum elastic modulus of mitral valve tissue from the collagen region (3697.2 ± 385.8 kPa anterior leaflet; 2582.1 ± 374.2 kPa posterior leaflet) ($p < 0.01$). However, the tensile elastic modulus measured from the toe region of the mitral valve stress-strain curves (532.8 ± 281.9 kPa anterior leaflet; 389.0 ± 156.9 kPa posterior leaflet) were not different than the Shore 27, Shore 35, and Shore 27 with Shore 35 blend TangoPlus material ($p > 0.95$). Shore 60 TangoPlus material was significantly stiffer than the toe region elastic modulus of mitral valves ($p < 0.05$).

Replication of the Subvalvular Apparatus

The geometries of the MV leaflets, annulus, papillary muscles and LV were successfully reconstructed from diastolic long-axis 3D TEE images (see Fig. 5b), whereas the chordae tendineae could not be accurately identified and replicated based solely on 3D TEE data. However, CT data permitted the detailed reconstruction of the subvalvular apparatus, including the chordae tendineae. To reconstruct the very fine and branched anatomy of chordae that do not appear in

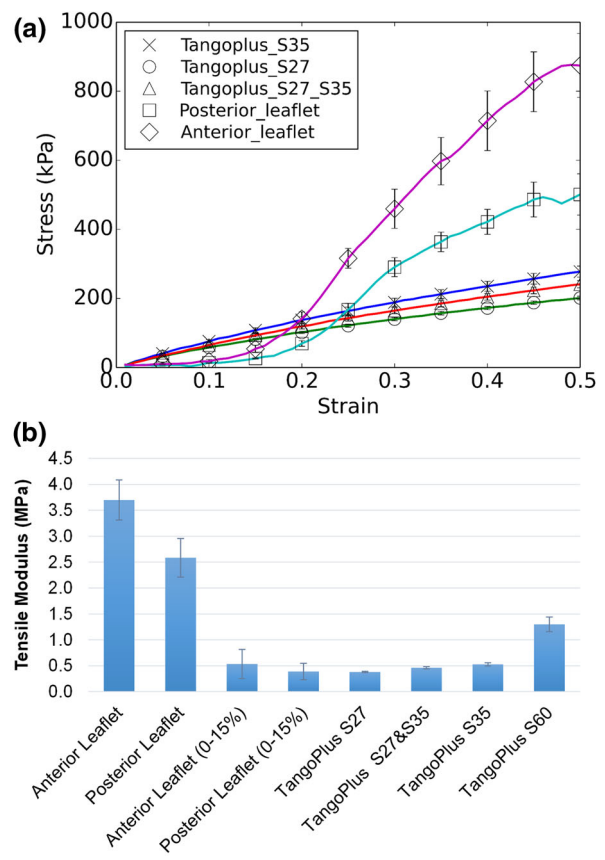


FIGURE 7. Results of mechanical testing of materials. (a) Stress vs strain of TangoPlus material ($n = 4$) compared to porcine mitral valve leaflets ($n = 3$) in uniaxial tension. In the toe region, the TangoPlus material demonstrates tensile mechanical response similar to valve tissue. (b) Comparison of tangent tensile modulus of TangoPlus material and mitral valve tissue. The maximum tangent modulus of valve tissue is significantly higher than the TangoPlus material ($p < 0.01$), but the modulus of the toe region of valve tissue is approximately the same as the TangoPlus materials. Higher shore values of TangoPlus material produced material with greater tensile modulus; shore 60 was significantly stiffer than the other TangoPlus materials ($p < 0.01$).

the single plane of CT images, it was necessary to tag the images in different views. Although the extraction of the chordae morphology was challenging, we were able to reconstruct their geometry and positions around the mitral leaflet coaptation zone. An example of the segmentation of the subvalvular anatomic data including the papillary muscles with chordae tendineae connected to the MV are shown in Fig. 6. 3D printing of the chordae tendineae has not been performed.

Benchmark Mitral Valve Repair Procedures

Patient-specific 3D printed MV models with pathological elements were utilized for the benchtop repair of two different MR clinical scenarios.

MitraClip Procedure

Reconstructed from 3D TEE images, a 3D printed model of the MV was used for the bench-top MitraClip procedure, shown in Fig. 8a. Fully open arms of MitraClip device were positioned perpendicular to the mitral coaptation line of the flexible dual-material model (see Fig. 8a, left panel), successfully approximating and grasping the valve leaflets. The deployed MitraClip device created a double opening orifice in the mitral valve model. After examining the structural integrity of the MitraClip device and the flexible leaflets we concluded that the MitraClip device remained static after pulling the device and forced distortion of the leaflets. Thus we concluded that the flexible TangoPlus is a suitable MV model material for MitraClip repair trial.

Mitral Valve Perforation Repair

Reconstructed from CT images, a 3D printed model of the MV with perforation and calcified depositions in the posterior leaflet was used for a bench-top repair employing a trans-catheter plug device. The geometry of mitral leaflets was accurately replicated, including the size, the shape and the location of perforation (see Fig. 8b). The length of the perforation in digital vs. physical model was 9.28 mm vs. 9.16 mm, the width

was 4.16 mm vs. 4.17 mm, the distance of the perforation from the posterior leaflet edge 9.96 mm vs. 9.40 mm, and distance of the perforation from the annulus was 9.26 vs. 9.21 mm, respectively. These measurements were vital in choosing the type and size of the most appropriate occluder device during the pre-procedural planning. The model permitted testing of several potentially suitable devices such as a combination of two Amplatzer Vascular Plug 4 (St. Jude Medical, St. Paul, Minnesota) devices that partially overlapped each other or the use of a single Amplatzer Duct Occluder (ADO) II (St. Jude Medical, St. Paul, Minnesota). After trying both types of devices the interventional cardiology team selected the Amplatzer Duct Occluder (ADO) II (see Fig. 8b) as the most favorable device and the most efficient option to fully occlude the leaflet perforation. The repaired MV model with the occluder positioned within the perforation is shown in Fig. 8b. Ultimately this modeling was used to guide a successful clinical repair procedure for this patient.⁵

DISCUSSION

We describe the creation of patient-specific 3D printed models of the mitral valve apparatus from

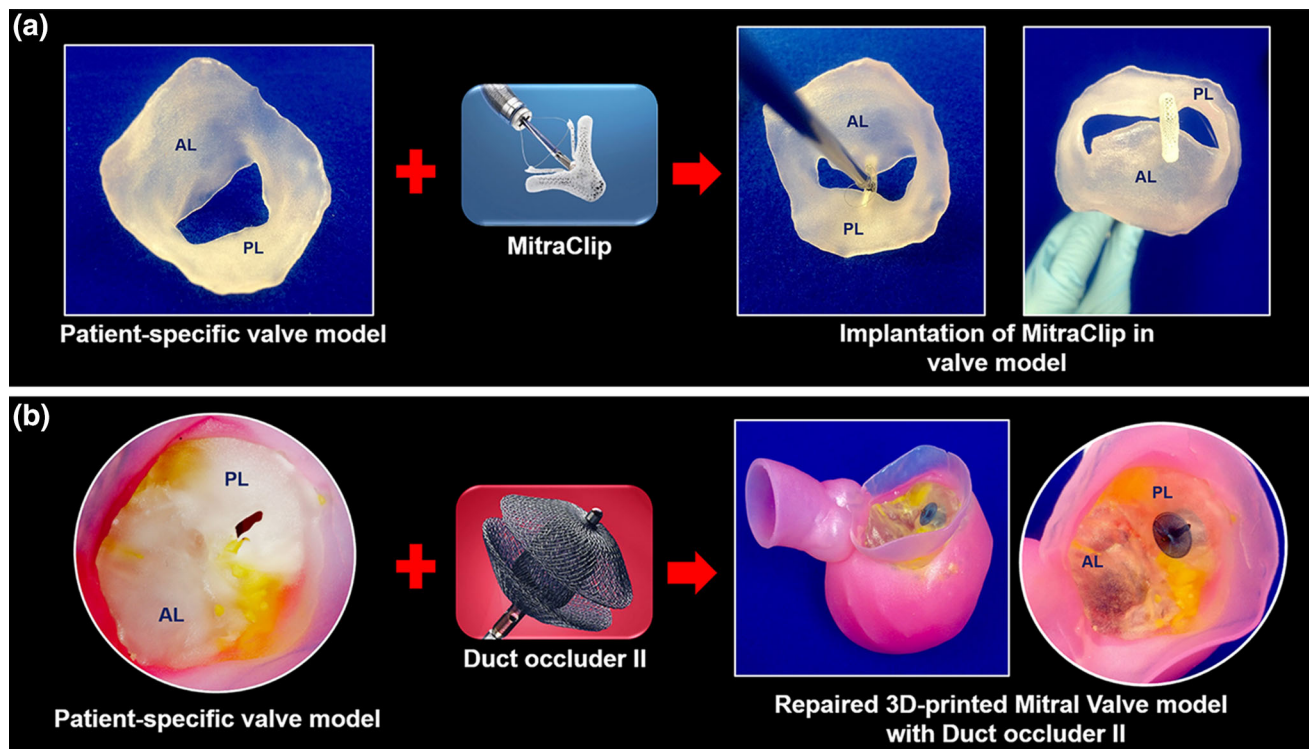


FIGURE 8. Planning the percutaneous mitral valve repair procedures. (a) Benchtop MitraClip procedure performed on patient-specific model of regurgitant MV. (b) MV perforation repair preprocedural planning; fitting the occluder into the perforation on the posterior leaflet.

medical imaging data. Our principal findings are that: (1) Both 3D TEE and CT imaging data can be used to replicate the morphology of the mitral leaflets, papillary muscles and LV, however CT is superior for the digital replication of chordae tendineae and pathologic calcification. (2) Multi-material 3D printing methods can be used to replicate the material properties of the mitral leaflets sufficiently well to permit implantation of catheter-based devices to repair MR.

Echocardiography is an attractive 3D printing image source for several reasons. It is widely available, cost-effective, requires no radiation, and is the primary imaging modality already in use to evaluate MR mechanism and severity. In addition 3D TEE is especially good at visualizing the mitral valve leaflets; provides functional valve information using spectral and color Doppler applications; and remains a highly focused imaging modality that generally captures only the anatomy of interest. Although Doppler methods can be used to derive an effective regurgitant orifice area, this concept has inherent limitations for the evaluation of device-valve interaction during both the systolic and diastolic phases of the cardiac cycle.

A specific concern for the use of 3D TEE imaging was whether or not the entire mitral apparatus could be captured within a single image dataset, or if two separately acquired image data sets could be combined within the digital modeling environment. In systole the mitral leaflets are closed and oriented perpendicularly to the chordae tendineae. The spatial resolution of ultrasound is highest along the axial imaging plane which restricts the ability to simultaneously capture fine anatomic detail of two structures aligned perpendicularly. As such the mitral leaflets are best imaged from a mid-esophageal en-face view whereas the chordae tendineae are best visualized from a ventricular long-axis view. We demonstrate that two separately acquired clinical 3D TEE image data sets can be fused within the digital IPS environment to overcome these axial resolution issues specific to ultrasound imaging.

Reconstruction and replication of calcium in the MV leaflets was more difficult from 3D TEE images than from CT images. Identification and digital tagging the mitral leaflet contours from 3D TEE data required careful optimization of imaging contrast and brightness, which could influence the accuracy and reproducibility of the 3D printed model. In contrast, CT data did not require any image quality adjustment prior to anatomic segmentation.

Although 3D TEE images may be digitally combined to improve the anatomic spatial resolution there are still significant limitations to using this imaging modality to replicate the mitral valve apparatus. As such, we felt it was important to compare our experi-

ence using either 3D TEE or cardiac CT imaging methods. The principal advantage of the CT images was the clear depiction of pathologic calcification around (or within) the MV apparatus, and the enhanced visualization of the chordae tendineae. The main limitations of the CT imaging approach to anatomic modeling are the need to expose the patient to ionizing radiation (a clinical concern for younger patients); the recognition that CT imaging is not usually performed for the clinical evaluation of mitral valve dysfunction; and the prolonged time required for segmentation of the very large anatomic data set captured by CT imaging. However this last limitation will likely be resolved as software advances will soon expedite the lengthy image segmentation process. Considering these advantages, whenever CT imaging is available it should be considered the imaging method of choice for reconstructing a 3D patient-specific MV model. However, in a case when a 3D TEE dataset is the only available imaging source, we showed that accurate and detailed reconstruction of MV, ventricle, LVOT and the papillary muscles is feasible.

Among many available 3D printing technologies, we chose to use PolyJet technology to fabricate the patient-specific models because it allows 3D printing of complex anatomical structures using multiple materials simultaneously. The PolyJet machine (Objet 500 Connex 3, Stratasys), creates objects by adding the successive layers with very high resolution (down to 16 μm), and allows the selection of print materials to target a range of material properties.

With this study our goal was to create geometrically accurate replicas of the mitral valve leaflets, to explore the digital reconstruction of the subvalvular apparatus; and to attempt bench-top catheter-based repair procedures on 3D printed patient-specific valve constructs. We chose to assign two different material properties to the mitral leaflet models. Healthy mitral leaflet tissue is heterogeneous and anisotropic in physical properties. The inner valve layer (spongiosa) being glycosylated and less-stiff than the atrial or ventricular outer layers of the leaflet. In contrast, our printed leaflet model was printed with a stiffer inner core since our principal goal was to create a valve with a softer external layer to optimize the physical interaction with a rigid repair device while maintaining the structural integrity of the printed leaflet under tension created by the device. For this study we successfully targeted our MV leaflet reconstruction to model the approximate stiffness of the toe region of the stress-strain curve (region of the physiological MV function),¹² and the transitional region in which the collagen fibers are recruited, with the strain less than 15%.

We demonstrate that the dual-material 3D printed valve construct of TangoPlus (Shore 27/Shore 35

combination) was similar to the 0–15% tensile modulus of the control leaflet tissue, however we recognize that replication of the multiple features and complexities of healthy or diseased mitral valve tissue will require significantly more effort and experimentation. For modeling the interaction of specific MV repair devices with the leaflet surface and surrounding tissues, the 3D printed material replication we describe was sufficient.

We learned that the time required to model such complex anatomy depends greatly on the image spatial resolution and visibility of the specific anatomy of interest within the imaging dataset, and on individual experience in imaging interpretation and data segmentation. After creating the 3D digital model an additional 12 h was typically required for the actual 3D printing process. Therefore the patient-specific model of the MV apparatus was delivered to the structural heart clinical team within 3 days.

Clinical Relevance

Clinically, our ability to predict intra-procedural challenges (such as difficult to grasp mitral leaflets) has been hampered by a lack of patient-specific MV models. The percutaneous MitraClip procedure is now a well-established method to achieve an edge-to-edge mitral valve repair, but as percutaneous MV replacement devices become available the best treatment option for a specific patient may not be clear. 3D anatomic modeling may provide a solution to determine the “best-fit” among all the possible catheter-based therapies soon to be available. In addition, such modeling may be valuable for predicting and potentially avoiding significant complications such as paravalvular regurgitation; device failure due to local calcification; or even the potentially devastating complication of LV outflow tract obstruction by the device or displaced native valve tissue. Our recent clinical experience has taught us that fused-material 3D modeling can be invaluable for pre-procedural device selection when there are patient-specific concerns about valvular calcification and its impact on the device landing zone on either surface of mitral valve leaflets.⁵ As catheter-based structural heart interventions become increasingly complex, the ability to effectively model patient-specific geometry as well as the interaction of an implanted device within that geometry will become ever more valuable.^{5,7,8}

The future prospects for such modeling efforts will likely focus on three ongoing needs. First, the accurate replication of the chordae tendineae will be needed to permit a robust evaluation of all trans-catheter mitral replacement devices currently being developed. Second, an increasingly sophisticated material blending

and texturization to improve the accuracy of replicated normal and diseased mitral leaflet physical properties. Third, the creation of functional 3D printed MV constructs that can be coupled to a flow loop to simulate patient-specific valve geometry and function.

CONCLUSION

In this study we report the principal finding that the mitral valve apparatus can be digitally reconstructed from currently available clinical imaging tools; that patient-specific mitral leaflet geometry can be accurately translated into physical multi-material 3D models; and that the material properties of such models are sufficient to simulate catheter-based mitral leaflet repair procedures.

REFERENCES

- ¹Durst, C. A., M. P. Cuchiara, E. G. Mansfield, J. L. West, and K. J. Grande-Allen. Flexural characterization of cell encapsulated PEGDA hydrogels with applications for tissue engineered heart valves. *Acta Biomater.* 7(6):2467–2476, 2011.
- ²Farooqi, K. M., and P. P. Sengupta. Echocardiography and three-dimensional printing: sound ideas to touch a heart. *J. Am. Soc. Echocardiogr.* 28(4):398–403, 2015.
- ³Goswami, R., C. Barker, N. Kleiman, M. Jackson, and S. H. Little. Transesophageal echocardiography-guided percutaneous intervention of a mitral valve leaflet perforation. *JACC Cardiovasc. Interv.* 8(5):754–755, 2015.
- ⁴Kheradvar, A., E. M. Groves, G. A. Simmons, B. Griffith, S. H. Alavi, R. Tranquillo, L. P. Dasi, A. Falahatpisheh, K. J. Grande-Allen, C. J. Goergen, M. R. K. Mofrad, F. Baaijens, S. Canic, and S. H. Little. Emerging trends in heart valve engineering: part III. Novel technologies for mitral valve repair and replacement. *Ann. Biomed. Eng.* 43(4):858–870, 2015.
- ⁵Little, S. H., M. Vukicevic, E. Avenatti, M. Ramchandani, and C. Barker. 3D Printed Modeling for Patient-specific mitral valve intervention: repair with a clip and a plug. *JACC Cardiovasc. Interv.* 9(9):973–975, 2016.
- ⁶Mahmood, F., K. Owais, C. Taylor, M. Montealegre-Gallegos, W. Manning, R. Matyal, and K. R. Khabbaz. Three dimensional printing of mitral valve using echocardiographic data. *JACC* 8(2):226–231, 2015.
- ⁷Maragiannis, D., M. S. Jackson, S. R. Igo, S. M. Chang, W. A. Zoghbi, and S. H. Little. Functional 3d printed patient-specific modeling of severe aortic stenosis. *JACC* 64(10):1066–1068, 2014.
- ⁸Maragiannis, D., Jackson, MS, S. R. Igo, R. C. Schutt, P. Connell, J. Grande-Allen, *et al.* Replicating patient-specific severe aortic valve stenosis with functional 3D modeling. *Circ. Cardiovasc. Imaging* 8(10):e003626, 2015.
- ⁹Merryman, W. D., H.-Y. S. Huang, F. J. Schoen, and M. S. Sacks. The effects of cellular contraction on aortic valve leaflet flexural stiffness. *J. Biomech.* 39(1):88–96, 2006.

- ¹⁰Nkomo, V. T., J. M. Gardin, T. N. Skelton, J. S. Gottdiener, C. G. Scott, and M. Enriquez-Sarano. Burden of valvular heart diseases: a population-based study. *Lancet* 368:1005–1011, 2006.
- ¹¹Olivieri, L. J., A. Krieger, Y. H. Loke, D. S. Nath, P. C. Kim, and C. A. Sable. Three-dimensional printing of intracardiac defects from three-dimensional echocardiographic images: feasibility and relative accuracy. *J Am Soc Echocardiogr.* 28(4):392–397, 2015.
- ¹²Richards, J. M., E. J. Farrar, B. G. Kornreich, N. S. Moise, and J. T. Butcher. The mechanobiology of mitral valve function, degeneration, and repair. *J. Vet. Cardiol.* 14:47e58, 2012.
- ¹³Witschey, W. R. T., A. M. Pouch, J. R. McGarvey, K. Ikeuchi, F. Contijoch, M. M. Levack, P. A. Yushkevich, C. M. Sehgal, B. M. Jackson, R. C. Gorman, and J. H. Gorman. Three-dimensional ultrasound-derived physical mitral valve modeling. *Ann. Thorac. Surg.* 98:691–694, 2014.